Hindawi
Advances in Civil Engineering
Volume 2020, Article ID 1763142, 16 pages
https://doi.org/10.1155/2020/1763142

Research Article

Performance of Special-Shaped Concrete-Filled Square Steel Tube Column under Axial Compression

Zhen Wang,[1] Xuejun Zhou ,[1] Fangshuai Wei,[1,2] and Mingyang Li[1,3]

[1]*School of Civil Engineering, Shandong Jianzhu University, Jinan, Shandong 250101, China*
[2]*School of Ocean Engineering, Dalian University of Technology, Dalian, Liaoning 116024, China*
[3]*General Technology Group Engineering Design Co. Ltd., Jinan, Shandong 250031, China*

Correspondence should be addressed to Xuejun Zhou; xuejunzhou@sdjzu.edu.cn

Received 15 January 2020; Revised 28 June 2020; Accepted 8 July 2020; Published 27 July 2020

Academic Editor: Filippo Ubertini

The axial compressive performance of novel L-shaped and T-shaped concrete-filled square steel tube (L/T-CFSST) column was assessed in this study. Ten L/T-CFSST columns were tested to failure under axial load. The experimental data were used to determine various failure modes, bearing capacities, and load-displacement curves. The test parameters included the section form, steel tube thickness, steel yield strength, and slenderness ratio. The axial compressive performance of the L/T-CFSST column proved favorable, and each square steel tube showed strong cooperative performance. The failure mode of the stub column specimen ($H/D \leq 3$) was strength failure caused by local buckling of the steel tube and that of the medium-long column member ($H/D > 3$) was instability failure caused by overall bending of the specimen. A finite element analysis (FEA) model was established and successfully validated by comparison against the test results. Based on the FEA model, parametric analyses were conducted to investigate the effects of steel tube thickness, concrete strength, steel yield strength, and slenderness ratio. The ultimate loads obtained from the experiments and FEA were compared to the results calculated by the available design codes. A formula was established to calculate the axial compressive strength and stability bearing capacity of the L/T-CFSST column accordingly. The calculation results are in close agreement with the FEA and experimental results, and the proposed formula may provide a workable reference for practicing engineers.

1. Introduction

Steel and concrete composite structures are widely used in civil engineering projects as they make full use of the superior material properties of steel and concrete [1]. The concrete-filled steel tube (CFST) column has high bearing capacity, high ductility, strong fire resistance, and good seismic performance; meanwhile, formwork is not needed, so CFST-based structures can be fabricated swiftly at relatively low cost [2]. These advantages make CFSTs popular in the civil engineering field and especially for prefabricated structures. Extensive theoretical research and laboratory experiments have revealed the mechanical properties of square and circle CFST columns, by Han et al. [3–7], Tao et al. [8–10], Güneyisi et al. [11], and Abed et al. [12], formed a comprehensive theoretical and specification system for CFSTs.

The steel column of traditional residential buildings is commonly a regular section. In this case, the column may protrude from the wall and affect the building's function [13]. Scholars have developed many different forms of special-shaped CFST (SS-CFST) columns to prevent this, including the SS-CFST column, the SS-CFST column with binding bars, with stiffener ribs, or connected by steel plates, and the multicell SS-CFST column, as shown in Figure 1, which can be embedded in the wall to avoid protrusions [14].

Recent researchers have conducted experimental and FEA investigations to probe the effects of various parameters on the compressive performance and seismic behaviors of SS-CFST columns. Lei et al. [15], Chen et al. [16], and Shen et al. [17] conducted axial and cyclic loaded tests on L-shaped and T-shaped CFST columns to establish axial compressive strength and stability bearing capacity

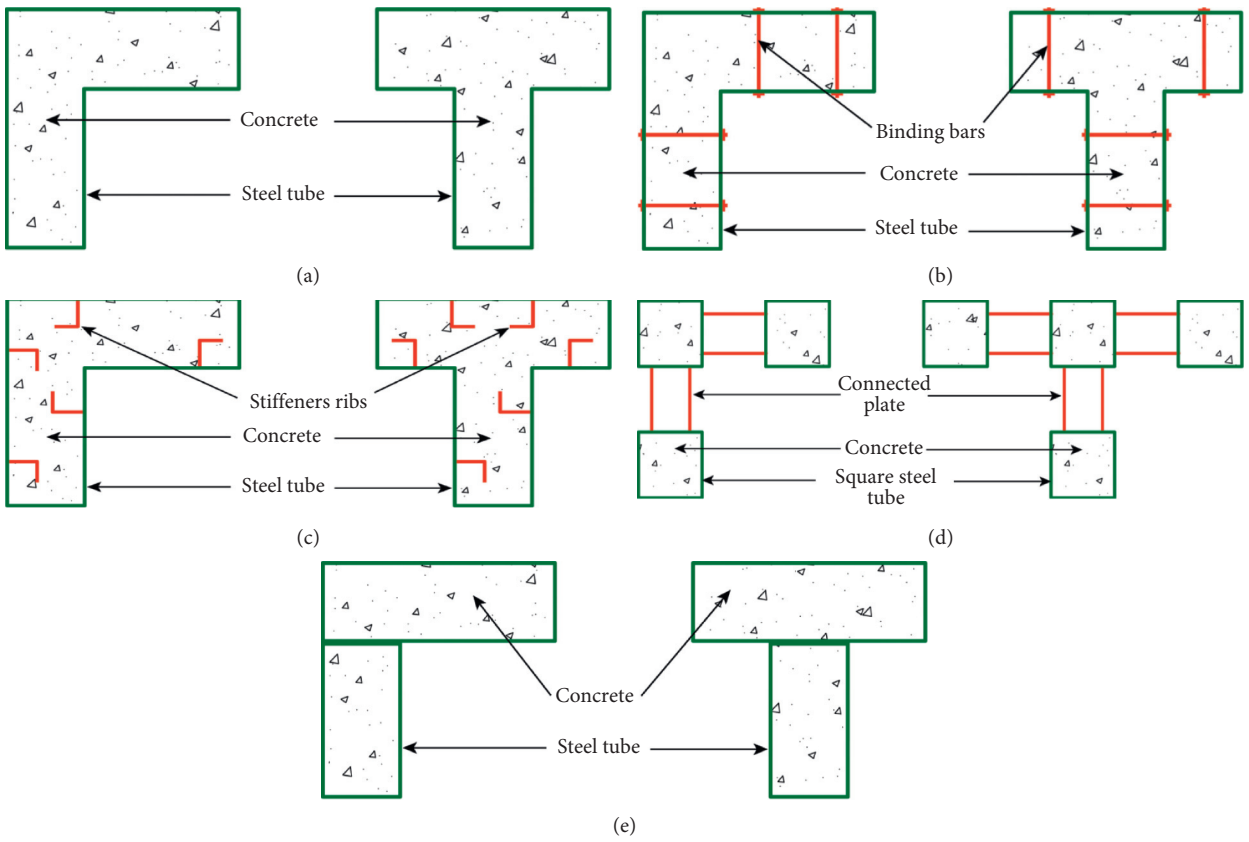

Figure 1: Cross-sections of special-shaped CFST columns: (a) SS-CFST column; (b) SS-CFST column with binding bars; (c) SC-CFST column with stiffener ribs; (d) SC-CFST column connected with steel plates; (e) multicell SC-CFST column.

calculation formulas. Experiment results indicated that the ductility of SS-CFST column was increased considerably by changing the local buckling mode of steel tube, and the inner corners almost failed to confine the concrete due to the separation between the steel tube and the core concrete. Zuo et al. [18–21] ran axial and eccentric compressive tests and cyclic loaded tests on T-shaped and L-shaped CFST columns with binding bars to deduce their bearing capacity calculation formulas. It was observed that the local buckling failure modes are changed, the occurrence of local buckling is delayed, and the global outward bulge of the steel tube at the concave corners can be effectively restrained by setting binding bars. In addition, the SS-CFST column with binding bars show higher lateral bearing capacity, higher stiffness, higher ultimate deformation capacity, and better energy-dissipation capacity compared with those without binding bars. Xu et al. [22], Liu et al. [23], and Tu et al. [24–26] subjected multicell composite L- and T-shaped CFST columns to axial compression and low cyclic loading tests; the results showed that the columns with multicell composite materials have good mechanical properties. Yang et al. [27, 28] carried out axial compression tests on eight stiffened T-shaped CFST columns and investigated the mechanical properties and failure modes of the specimens. It was found that the stiffeners improve the ductility and the peak resistance of T-shaped CFST column substantially. Xiong et al. [29–32] and Xu et al. [33, 34] systematically analyzed the mechanical properties of SS-CFST columns connected by different battens and established the bearing capacity calculation formulas corresponding to different stress states.

However, there are some unresolved problems related to SS-CFST columns including the stress concentration at the internal and external corners, complex connection structure, and large amounts of welding and residual welding stress. These problems must be solved to satisfy the requirements of prefabricated steel residential buildings. In China, some prefabricated steel structure residential buildings adopt novel special-shaped concrete-filled steel square tube columns. The novel special-shaped column is composed of many manufactured square steel tubes connected via structural weld at the chamfer of the square steel tube in the factory and then combined into L-shape, T-shape, and crisscross-shape sections poured with concrete at the construction scene. The section form is shown in Figure 2. Compared with ordinary SS-CFSTs, the manufactured square steel tube can be purchased directly from the factory; this mitigates the difficulties brought on by traditional thick steel plate cold bending and welding, reduces the welding residual stress and residual deformation, and better meets the construction accuracy requirements for fabricated steel buildings.

In order to study the performance of the novel special-shaped CFST column under axial compression, ten L/T-CFSST column specimens were tested under axial load

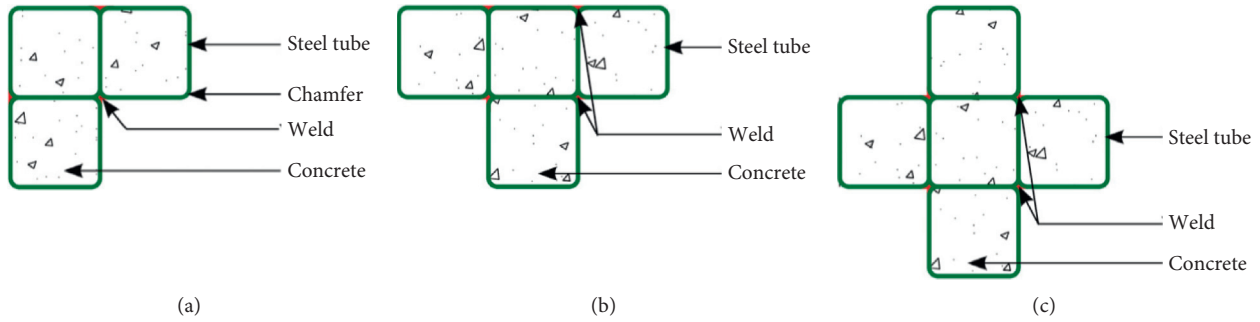

Figure 2: Novel special-shaped CFST column sections. (a) L shape. (b) T shape. (c) Crisscross shape.

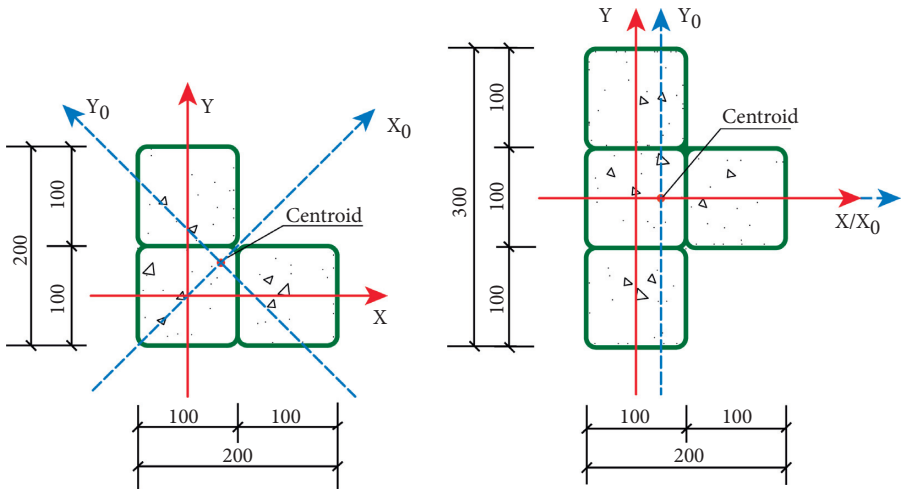

Figure 3: Cross-section of specimens.

Table 1: Specimens in detail.

Specimen	Steel grade	H (mm)	D (mm)	H/D	t (mm)	λ_{x0}	λ_{y0}	α	ξ	N_{uT} (kN)	N_{uFEA} (kN)	N_{uFEA}/N_{uT}
L-1	Q235	600	200	3	4	9	12	0.18	1.4	2620	2363	0.90
L-2	Q355	600	200	3	4	9	12	0.18	2.1	3288	2999	0.91
L-3	Q235	600	200	3	6	9	12	0.29	2.3	3055	2909	0.95
L-4	Q235	900	200	4.5	4	13	18	0.18	1.4	2403	2211	0.92
L-5	Q235	1200	200	6	4	17	24	0.18	1.4	2239	2151	0.96
T-1	Q235	900	300	3	4	11	16	0.18	1.4	3140	3159	1.00
T-2	Q355	900	300	3	4	11	16	0.18	2.0	3808	3978	1.04
T-3	Q235	900	300	3	5	11	16	0.23	1.8	3817	3734	0.98
T-4	Q235	1200	300	4	5	15	21	0.23	1.8	3580	3521	0.98
T-5	Q235	1500	300	5	5	19	26	0.23	1.8	3350	3297	0.98

conditions with varying parameters including section form, steel tube thickness, steel yield strength, and slenderness ratio. The failure modes, bearing capacities, and load-displacement curves of the specimens were analyzed accordingly. Corresponding FEA models were established. Parametric studies were carried out based on the FEA models to establish the bearing capacity calculation formula for L/T-CFSST columns based on modification of the AIJ code. The calculation results were in close agreement with both FEA and experimental results, which suggests that the proposed model may provide a workable reference for practicing engineers and designers.

2. Experimental Research

2.1. Specimen Design and Manufacture. Ten L/T-CFSST columns were tested under axial compression to observe the effects of various parameters including the section form, steel tube thickness and strength, and slenderness ratio. Figure 3 and Table 1 list the geometric and sectional dimensions of the specimens. In Table 1, H refers to the height of the column, D is the maximum width of the section of the test piece, t is the thickness of the steel tube, λ_{xo} and λ_{yo} are the slenderness ratio of the column around the X_0 and Y_0 axis, respectively. α means the steel ratio of the

Table 2: Mechanical properties.

Material	t (mm)	f_y (MPa)	f_u (MPa)
Steel Q235	4	320.5	480.6
Steel Q235	5	390.0	488.3
Steel Q355	4	456.7	546.7

cross–section, and ξ is the confinement factor. The calculation formula for these parameters is

$$\lambda = \frac{H}{i},$$
$$i = \frac{\sqrt{E_s I_s + 0.2 E_c I_c}}{\sqrt{E_s A_s + 0.2 E_c A_c}},$$
$$\alpha = \frac{A_s}{A_c}, \quad (1)$$
$$\xi = \alpha \cdot \left(f_y / f_{ck}\right),$$

where i is the turning radius of the cross-section, E_s, I_s, E_c, and I_c are the elastic modulus and the moment of inertia of steel and concrete, respectively, A_s and A_c are the section area of steel tube and concrete, f_y is the yield stress of steel, and f_{ck} is the characteristic strength of concrete.

The test specimens consist of three parts: the L/T-CFSST column, a top cover plate, and a bottom cover plate. When processing L/T-CFSST columns, the steel tube was first cut down according to the design length and positioned according to the section form. The steel tube chamfer was welded, and then the steel cover plate at the bottom of the specimen was welded. Self-compacting concrete was poured into the square steel tube and cured. The upper part of the specimen was grinded, and the top cover plate was welded to ensure that the steel tube and core concrete would bear force simultaneously throughout the test. Air vent holes were reserved in the steel tubes to ensure fully compacted concrete.

2.2. Mechanical Properties. Standard tensile tests on coupons were conducted to measure the material properties of the steel tubes. The measured average yield strength (f_y), ultimate strength (f_u) are listed in Table 2, and the elastic modulus of steel (E_s) is 206 GPa. The core concrete of L/T-CFSST column is poured by commercial concrete, and the mix proportions of the concrete are as follows: cement: 280 kg/m^3; river sand: 700 kg/m^3; water: 156 kg/m^3; fly ash: 100 kg/m^3; coarse aggregate: 1150 kg/m^3; and additional high range water reducer (HRWR): 6.3 kg/m^3. The average measured compressive cube strengths (f_{cu}) of the concrete at the time of testing were 38.44 MPa, and the values of elastic modulus (E_c) for the concrete were 30 GPa.

2.3. Loading Devices and Procedure. The test was carried out on a 5000 kN computer-controlled servo-hydraulic universal testing machine, and the experimental devices are depicted in Figure 4. A knife-edge articulation system was

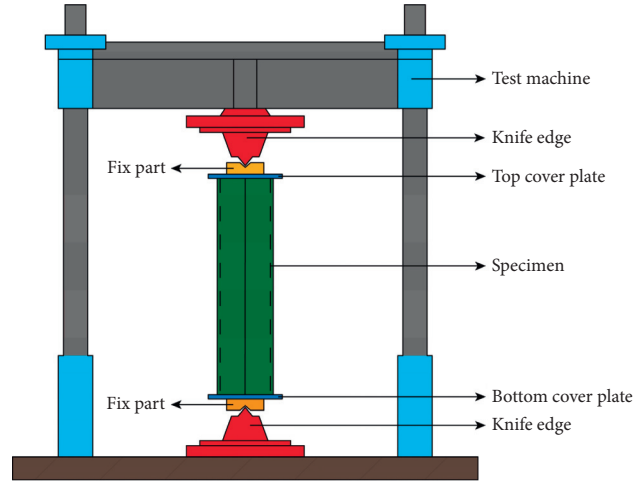

Figure 4: Loading devices.

sandwiched between press machine and specimen to simulate top and bottom articulated boundary conditions. The knife-edge articulation system consists of two parts: fix part and knife-edge. The fixed part is welded on the cover plate, the knife-edge passes through the centroid of the L/T-CFSST column specimen and coincides with the Y_0 axis, and the load line is applied on the fixed part through the knife-edge to realize the axially loading.

The force-controlled mode was adopted at the beginning of the loading process. The subsequent loading speed was 100 kN/min. Once the load-vertical displacement curve changed from a straight line to a curve, the device was switched into displacement-controlled loading mode and the loading speed was controlled at 0.5 mm/min. The axial load-vertical displacement curve was directly obtained from universal testing machine. Linear variable displacement transducers (LVDTs) were arranged at three divided points of the specimen to monitor the lateral displacement. Strain gauges were attached to the midheight cross-section of each surface to measure longitudinal and horizontal strains. Surfaces and strain gauges number and instrumentation layout are shown in Figure 5.

3. Test Phenomena and Discussion

3.1. Test Phenomena. According to the height of L/T-CFST column, the test phenomena can be divided into two categories. For the stub column ($H/D \leq 3$) [35], during the initial loading period, the specimen was in the elastic stage and presented no obvious phenomenon; the steel tube and concrete were independently subjected to the load. As the load increased, the specimen made a sound, and the load growth rate slowed down. Local buckling occurred on the surface of the steel tube, and the degree of buckling increased as the axial load increased. After reaching the ultimate bearing capacity, the specimen entered the failure stage, the axial load began to decrease, and serious local buckling occurred across the steel tube surface. The specimen finally bent around the Y_0 axis upon failure of steel tube after local buckling. It is worth noting that the universal testing

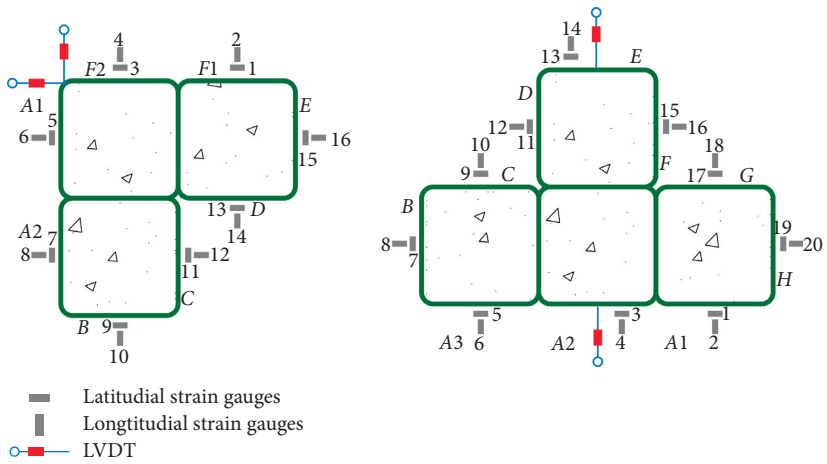

Figure 5: Surfaces, strain gauge number, and instrumentation layout.

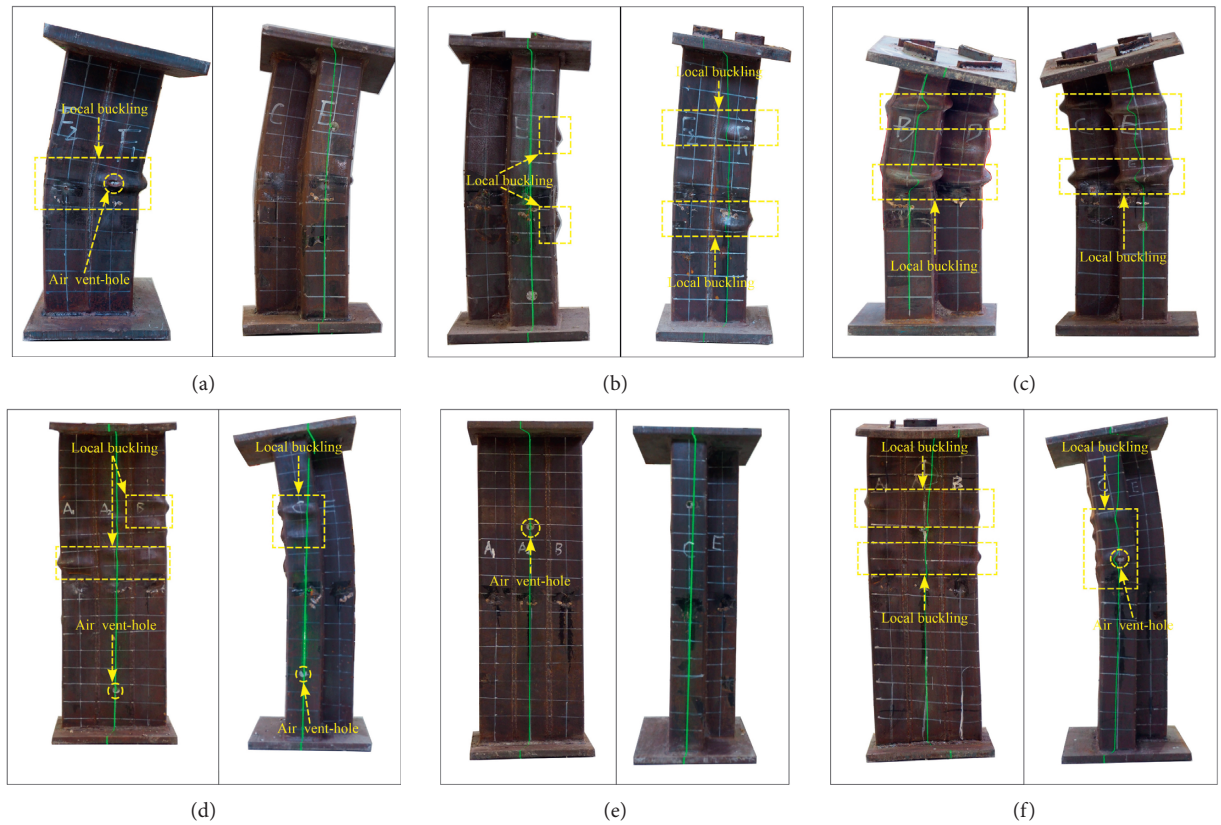

Figure 6: Failure characteristics of stub columns: (a) L-1; (b) L-2; (c) L-3; (d) T-1; (e) T-2; (e) T-3.

machine leaked oil during the T-2 specimen test, so the test data of T-2 was incomplete. The final failure characteristics of stub columns are shown in Figure 6.

There was no obvious phenomenon observable in the medium-long column from the beginning of loading to 80% of the ultimate load. As loading continued, the specimen began to show slight bending deformation. The lateral deformation grew more obvious as the loading increased until the steel tube of the L-CFSST column presented local buckling. Upon reaching the ultimate bearing capacity, the bearing capacity dropped off as lateral deformation continued to increase until overall bending occurred along the Y_0 axis and the specimen was significantly damaged. The final failure characteristics of the medium-long column are shown in Figure 7.

3.2. Failure Mode. The axial compression process of the L/T-CFSST column can be divided into three stages as per the test phenomena observed here: the elastic stage, the elastic-plastic stage, and the failure stage. There is no obvious

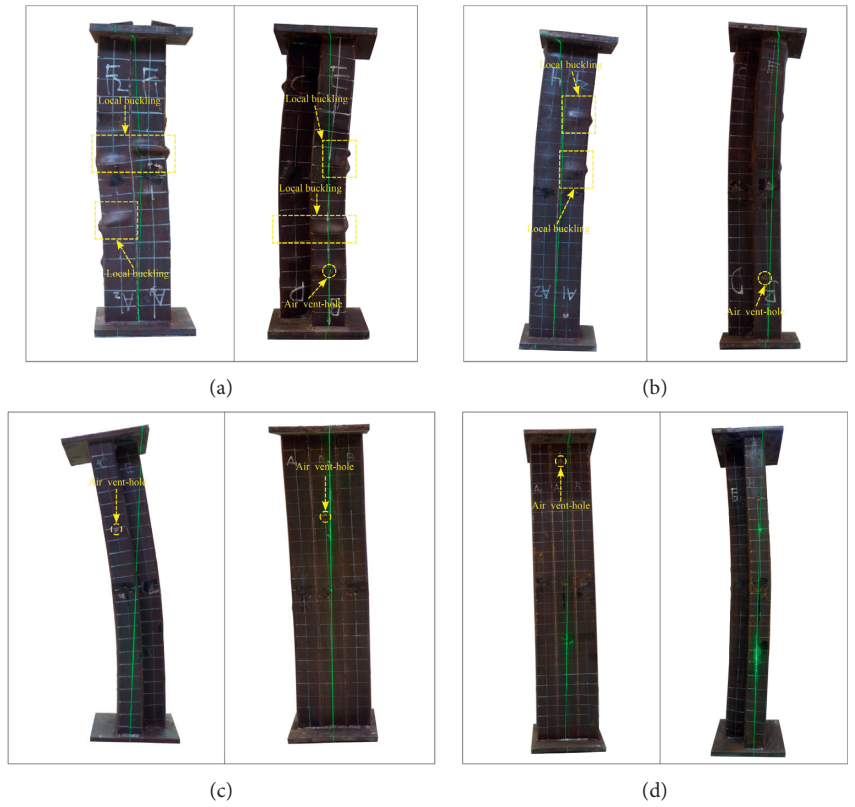

Figure 7: Failure characteristics of medium-long columns: (a) L-4; (b) L-5; (c) T-4; (d) T-5.

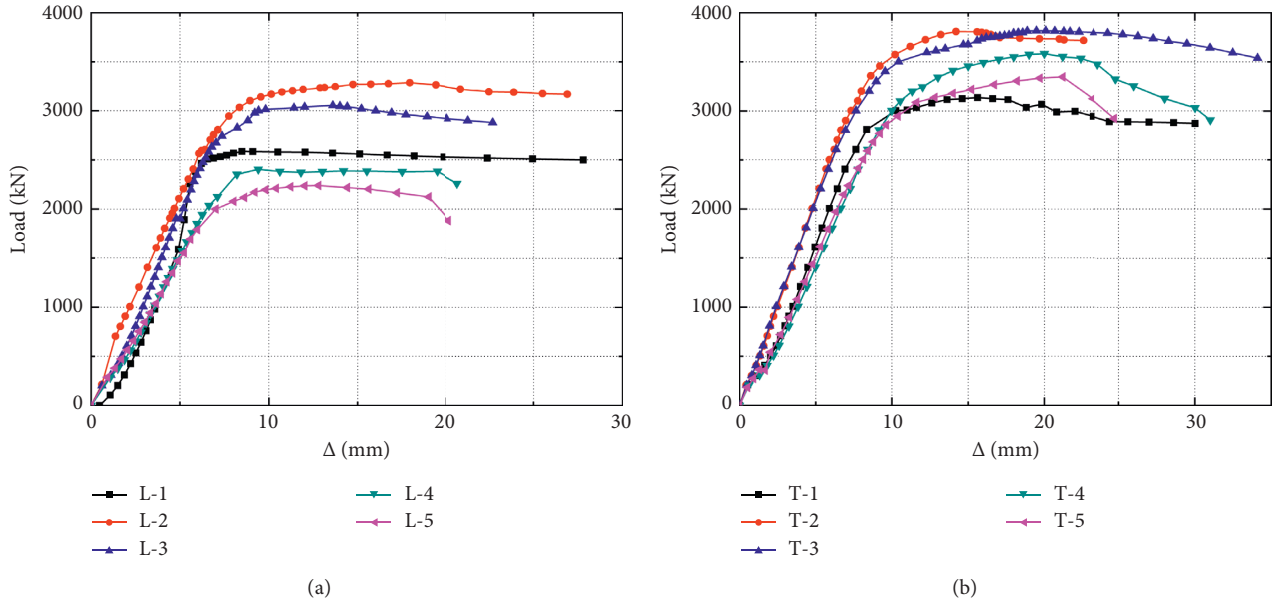

Figure 8: Axial load (P)-vertical displacement (Δ) curves: (a) L-shaped column; (b) T-shaped column.

phenomenon in the elastic stage, the steel tube and concrete bear the load separately, and the combined action of the steel tube and concrete has not yet occurred. In the elastic-plastic stage, the steel tube restrains the concrete once the horizontal deformation of concrete exceeds the horizontal deformation of the steel tube. At this time, the concrete is in a state of triaxial compression and the steel tube can be regarded as the plane stress state of axial compression and circumferential tension. As the load further increases, the steel tube yields under compression and local buckling or

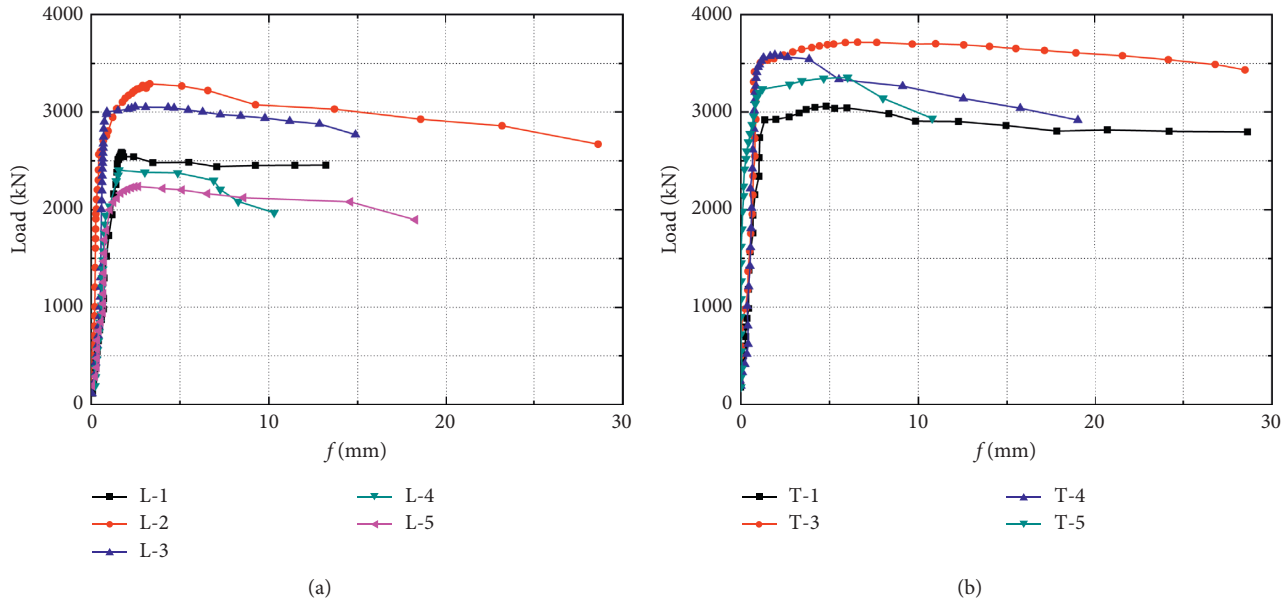

Figure 9: Axial load (P)-lateral displacement (f) curves: (a) L-shaped; (b) T-shaped.

bending deformation can be observed. In the failure stage, the concrete is crushed and the bearing capacity of the specimen is markedly reduced. The strength failure caused by local buckling of the steel tube characterizes the failure mode of stub columns. For medium-long columns ($H/D > 3$), the failure mode observed here was instability failure caused by overall bending of the specimen. It is worth noting that there was no cracking or separation in the weld between steel tubes during this tests run in this study; the L/T-CFSST column showed strong cooperative performance.

3.3. Axial Load-Vertical Displacement Relationships. Figure 8 presents the axial load (P)-vertical displacement (Δ) curves of the specimens. All such curves share similar shapes within which three stages (elastic, elastic-plastic, and failure) can be clearly identified. In the elastic stage, the P-Δ curve forms basically a straight line. Upon entering the elastic-plastic stage, the steel tube yields, the axial compression rigidity of the specimen decreases, and the resulting curve shows obvious nonlinearity.

According to Table 1 and Figure 8, the bearing capacities of L-2 and L-3 were higher than those of L-1 while those of T-2 and T-3 were higher than those of T-1, indicating that the bearing capacity can be improved by adjusting the strength and thickness of the steel tube. As per the L-1, L-4, L-5 and T-3, T-4, T-5 curves, the column height increased as the ultimate load of the specimen decreased. In the failure stage, the bearing capacity of the medium-long column decreased rapidly after the instable failure occurred, and the slope of its P-Δ curve is much higher than that of the stub columns. This is because the additional bending moment increased with the slenderness ratio while the bearing capacity decreased with the second-order effect. This suggests that the slenderness ratio influences the bearing capacity and failure mode of the column.

3.4. Axial Load-Lateral Displacement Relationships. The axial load (P)-lateral displacement (f) of the midheight curve is shown in Figure 9. In the elastic stage, the curve forms basically a straight line and the relationship between P and f is linear. The load increased rapidly in this stage while the lateral displacement was small. In the elastic-plastic stage, the rigidity of the specimen appears to decrease as the lateral displacement increases with the load; the slope of the P-f curve decreases over a nonlinear relationship. The L-1, L-2, L-3 and T-1, T-3 curves show that, under the same axial load, the rigidity and the peak load of any specimen with higher strength and a thicker steel tube are larger while the lateral deflection is smaller. The L-1, L-4, L-5 and T-3, T-4, T-5 curves similarly show that the rigidity and peak load of the specimens with larger slenderness ratios are smaller and the lateral deflection is larger. These results altogether suggest that lateral deformation can be limited by increasing α and ξ.

4. Finite Element Modeling

4.1. Element Types. To further analyze the influence of individual parameters on the axial bearing capacity of the L/T-CFSST column, a three-dimensional (3D) FEA model was established in ABAQUS software. In the FEA model, the cover plate was simulated by a rigid body, the square steel tube was simulated by a 4-node shell element with a reduced integral (S4R), and the concrete was simulated by 8-node brick elements with reduced integration (C3D8R).

4.2. Boundary Conditions and Load Application. The boundary conditions of each FEA model were the same as those in the test. The coupling point was specified at the centroid of the cover plate. The coupling point of the top cover plate was constrained in the X and Z displacement directions, and the displacement of the coupling point of

bottom cover plate was restricted in all three directions. The welds among steel tubes and between steel tube and cover plate are simulated by "Tie" interactions. The interface model of the steel tube and concrete was composed of two parts: tangential sliding and normal contact. The Coulomb friction model was imposed along the tangent of the contact surface. The interface friction coefficient was taken as 0.6, as recommended by Han et al. [2]. A hard contact was set along the normal direction of the contact surface, which allows for separation of materials but does not mutual penetration. The load was applied as a static vertical load using the displacement control at the coupling point of the top cover plate (identical to the experimental test). The initial geometric imperfection of the samples was considered to be $L/1000$.

4.3. Material Properties. The stress-strain relationship of steel tube adopts the simplified bilinear model. The yield stress and elastic Young's modulus obtained from tensile coupon test were employed in the analysis. The elastic modulus of the strengthened section in this case was $0.01E_s$ and Poisson's ratio was taken as 0.3.

To describe the compressive performance of the core concrete, an equivalent stress (σ)-strain (ε) model was proposed by Wang et al. [21] (equation (2) was used with the σ-ε model for core concrete tensile properties (equation (3)):

$$y = \begin{cases} 2 \cdot x - x^2, & (x \le 1), \\ \dfrac{x}{\beta_0 \cdot (x-1)^{\eta} + x}, & (x > 1), \end{cases} \tag{2}$$

$$\sigma_t = \begin{cases} E_c \varepsilon_t, & (0 \le \varepsilon_t < 0.1 f_c'/E_c), \\ f_c' \left[0.1 - \dfrac{10}{9} \left(\varepsilon_t - 0.1 \dfrac{f_c'}{E_c} \right) \right], & (\varepsilon_t > 0.1 f_c'/E_c), \end{cases} \tag{3}$$

where $x = \varepsilon/\varepsilon_0$, $y = \sigma/\sigma_0$, and $\sigma_0 = f_c'$. β_0 and ε_0 are parameters related to the passive confinement provided by the steel tube to the concrete, $\beta_0 = (f_c')^{0.1}/[1.2 \times (1+\xi)^{0.5}]$, $\varepsilon_0 = \varepsilon_c + 800 \times \xi^{0.2} \times 10^{-6}$, $\varepsilon_c = (1300 + 12.5 \times f_c')10^{-6}$, $\eta = 1.6 + 1.5/(x.f_c')$ is the cylinder compressive strength of concrete, E_c is the elastic modulus of concrete ($4700 \times (f_c')^{0.5}$ here), and Poisson's ratio of concrete is 0.2 under ACI [36].

A damaged plastic model was used to simulate the concrete where in the key parameters include the dilation angle (ψ), flow potential eccentricity (ef), ratio of the biaxial compression strength to uniaxial compression strength of concrete (f_{b0}/f_{c0}), ratio of the second stress invariant on the tensile meridian to that on the compressive meridian (K), and viscosity parameter of 30°, 0.1, 1.16, 2/3, or 0, respectively [37].

4.4. Verification of Finite Element Model. Table 1 shows a comparison between the peak load N_{uT} from the test and the peak load N_{uFEA} from the FEM. The average value of N_{uFEA}/N_{uT} is 0.96, and the two sets of results are similar. A comparison between the failure characteristics of L-1 specimen obtained by finite element analysis versus the test is shown in Figure 10. It can be seen that the failure pattern obtained by finite element analysis was basically consistent that by with test. The axial load-maximum strains curves obtained from the finite element model (FEM) and the tests on L/T-CFSST column specimens were compared as shown in Figure 11. It is observed that the FEM strains are in accordance with the test results in the elastic stage; the curves are nearly coincident. In the elastic-plastic stage and the failure stage, the FEM and test curves are not as close but have reasonable accuracy. This comparison further verifies the accuracy of the FEA. It can be concluded that the finite element analysis model established in this paper can accurately reflect the axial compression characteristics of the L/T-CFSST column.

4.5. Parametric Analysis. A series of parametric analyses were carried out to investigate the behaviors of L/T-CFSST column subjected axial load. The effects of steel thickness, steel strength, concrete strength, and slenderness ratio on the structural performance of axially loaded columns in terms of the load-displacement curves were assessed for each specimen. The numbering rules of specimen in the parameter analysis are shown in Figure 12.

4.5.1. Effect of Steel Thickness. Figure 13 shows the effect of steel tube thickness on the load (P)-vertical displacement (Δ) of the L/T-CFSST stub column. In the elastic stage, a greater specimen thickness (with the same column height) results in greater axial compressive rigidity and higher ultimate bearing capacity. In the failure stage, the restraining effect of the steel tube on the core concrete appears to be enhanced by tube thickness, which slowly reduces the bearing capacity and creates a gentler P-Δ curve.

4.5.2. Strength Effect of Concrete. The effects of concrete strength on the load (P)-vertical displacement (Δ) curves for L/T-CFSST stub columns were assessed as shown in Figure 14. The curves basically coincide in the elastic stage, indicating that changing the concrete strength has little impact on the initial compressive rigidity. After entering the plastic stage, the bearing capacity appears to increase as the concrete strength increases. In the failure stage, the greater the strength of concrete, the faster the bearing capacity decreases, and stronger concrete shows a faster decrease in bearing capacity. This is because the load on core concrete after crushing is mainly borne by the steel tube.

4.5.3. Strength Effect of Steel Tube. The load (P)-vertical displacement (Δ) curves of L/T-CFSST stub columns with different steel strengths are shown in Figure 15. Changes in steel strength appear to have little effect on the axial compressive rigidity of these specimens. Higher steel strength suggests stronger restraint of the steel tube to the core concrete. The P-Δ curve becomes more gentle in the failure

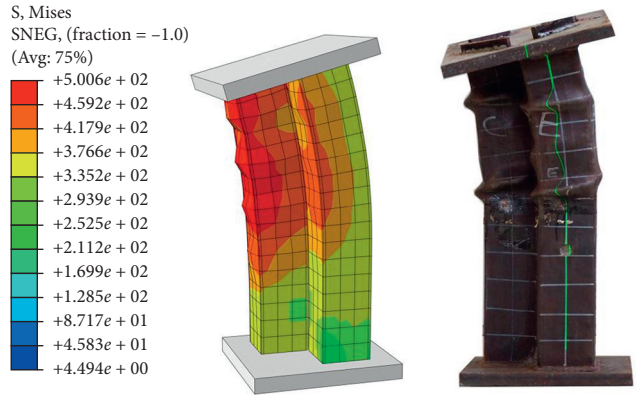

Figure 10: Comparison of L-3 specimen failure mode between FEM and test.

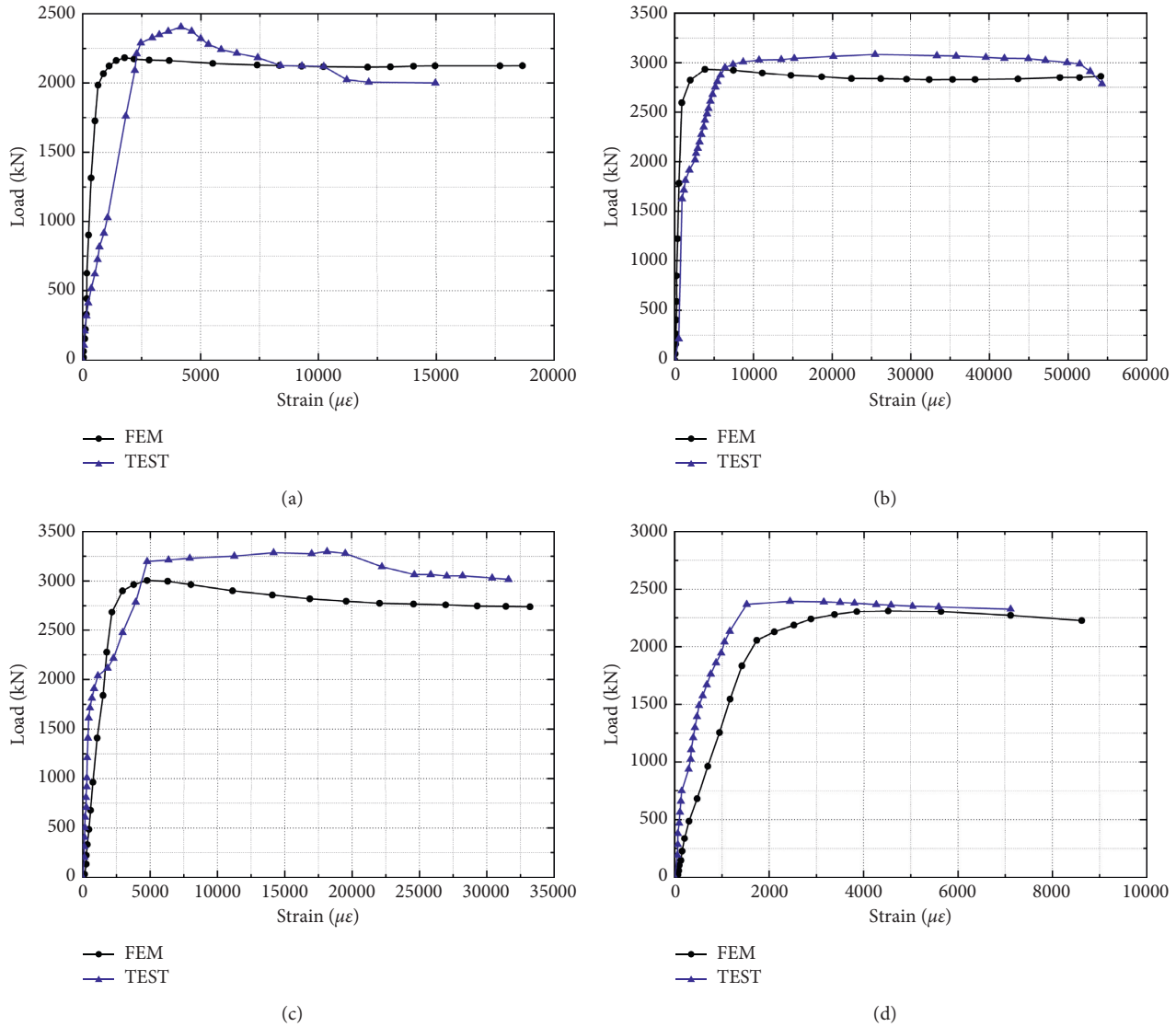

Figure 11: Continued.

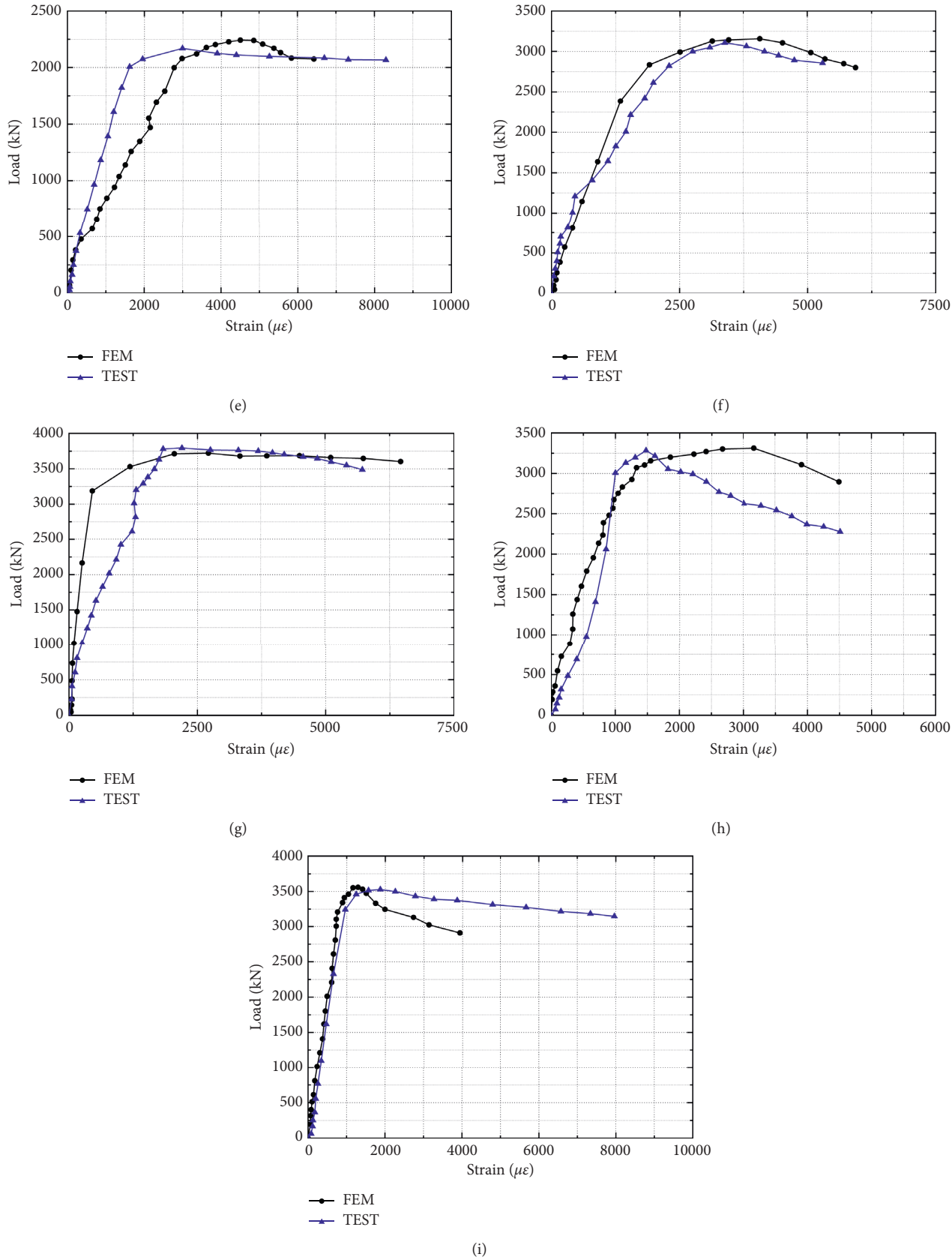

Figure 11: Comparison of axial load-maximum strain curves between FEM and test: (a) L-1; (b) L-2; (c) L-3; (d) L-4; (e) L-5; (f) T-1; (g) T-3; (h) T-4; (i) T-5.

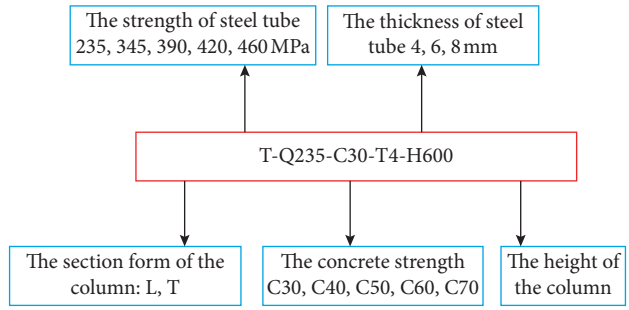

Figure 12: Specimen naming rule.

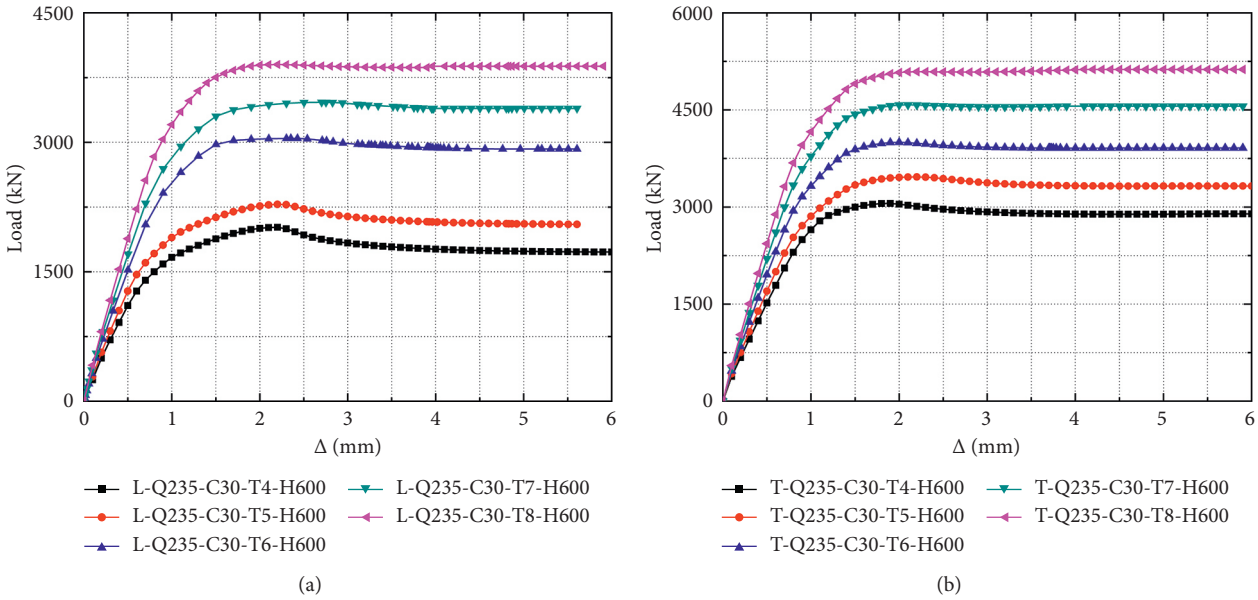

Figure 13: Load-vertical displacement curves of steel tubes with different thickness: (a) L-shaped; (b) T-shaped.

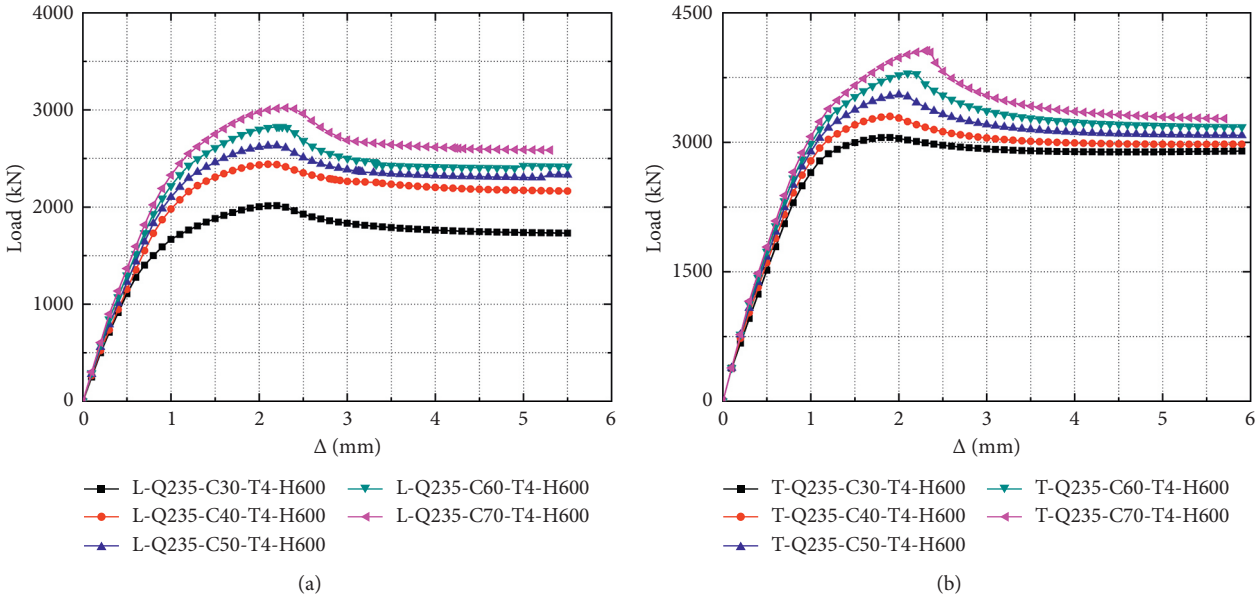

Figure 14: Load-vertical displacement curves of concrete with different strengths: (a) L-shaped; (b) T-shaped.

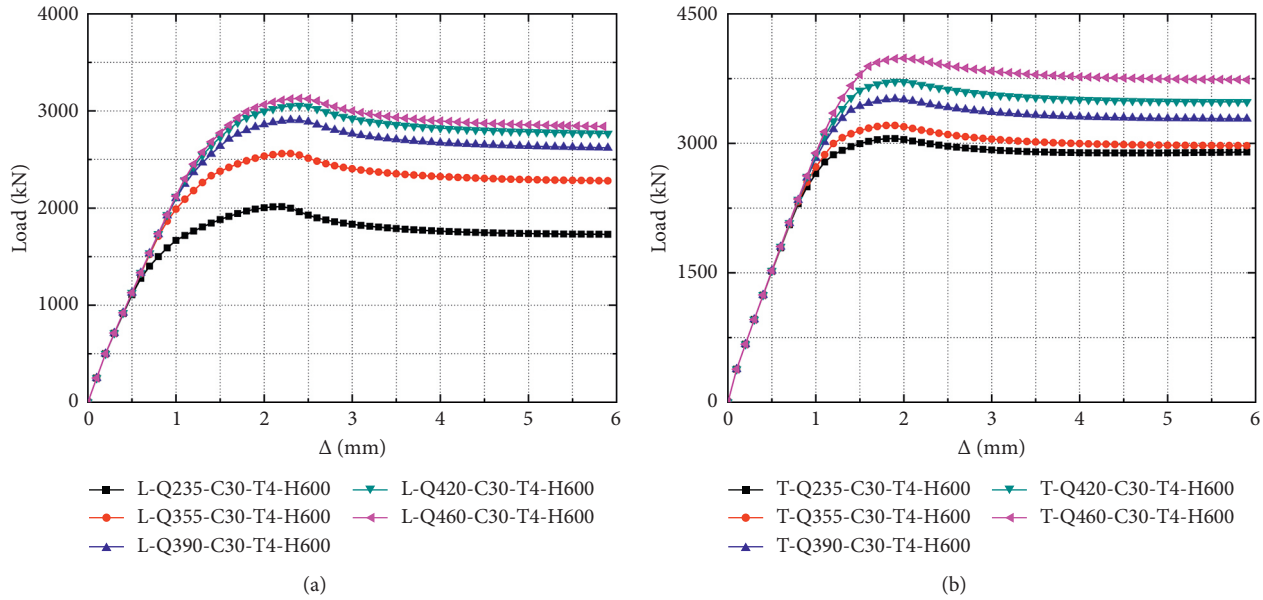

Figure 15: Load-vertical displacement curves of the steel tubes with different strengths: (a) L-shaped; (b) T-shaped.

stage as the ultimate bearing capacity of the specimen increases.

4.5.4. Steel Tube Slenderness Ratio. According to the experimental phenomena and other data provided in Table 1, the slenderness ratio significantly influences the failure mode and bearing capacity of L/T-CFSST columns; the slenderness ratio must be considered when calculating the bearing capacity. The influence of slenderness ratio on the load (P)-vertical displacement (Δ) curve of the specimens was assessed as shown in Figure 16. It appears that the bearing capacity of specimens with small slenderness ratios slowly declines, producing a flat P-Δ displacement curve indicative of good ductility performance. The bearing capacity of the large-slenderness-ratio specimen decreases faster, showing the characteristics of instability failure.

5. Calculating L/T-CFSST Column Bearing Capacities

5.1. Strength Bearing Capacity. The main specifications for CFST column bearing capacity calculation subjected axially load include BS 5400 [38], AISC 360-05 [39], EC 4 [40], AIJ [41], CECS 159 [42], GJB 4142-2000 [43], and DBJ/T 13-51-2010 [44]. The specific calculation methods for square CFST columns are introduced below.

The calculation for the ultimate bearing capacity of CFST specified in BS5400 (2005) is based on the superposition theory. The contribution of steel and concrete is appropriately reduced. The equation for the ultimate axial compressive bearing capacity of the square CFST column is

$$N_u = 0.95A_s \cdot f_y + 0.45A_c \cdot f_{cu}, \tag{4}$$

where N_u is the ultimate axial compressive bearing capacity of the square CFST, A_s and f_y are the cross-sectional area and yield strength of the steel tube, and A_c and f_{cu} are the cross-sectional area and the cube compressive strength of concrete, respectively.

As specified in ANSI/AISC 360-05, the rectangular CFST column calculations are as follows:

$$\begin{aligned}
N_u &= \left[0.658\left(\frac{N_0}{N_{cr}}\right)\right] \cdot N_0 \text{when} \quad \left(N_{cr} \geq 0.44N_0\right),\\
N_u &= 0.877N_{cr} \text{when} \quad \left(N_{cr} < 0.44N_0\right),\\
N_0 &= A_s \cdot f_y + C_1 \cdot A_c \cdot f_c',\\
N_{cr} &= \frac{\pi^2\left(E_s \cdot I_s + C_2 \cdot E_c \cdot I_c\right)}{(K \cdot L)^2},\\
C_2 &= 0.6 + \frac{2A_s}{\left(A_s + A_c\right)} \leq 0.9,
\end{aligned} \tag{5}$$

where N_u is the nominal compressive bearing capacity, N_{cr} is the elastic critical buckling bearing capacity, N_0 is the nominal axial compressive strength without consideration of slenderness ratio, A_s, f_y, and E_s are the cross-sectional area, yield strength, and elastic modulus of the steel tube, A_c, f_c', and E_c are the cross-sectional area, the cylinder compressive strength, and the elastic modulus of concrete, respectively, I_s and I_c are the moment of inertia of the steel section and the concrete section about the elastic neutral axis, C_1 equals 0.85, C_2 is the coefficient for calculation of effective bending stiffness, and K is the effective length factor.

Under EC 4 (2005), the strength of axially loaded square CFST columns is determined by summing the strength values of the steel tube and concrete. The axial load-carrying

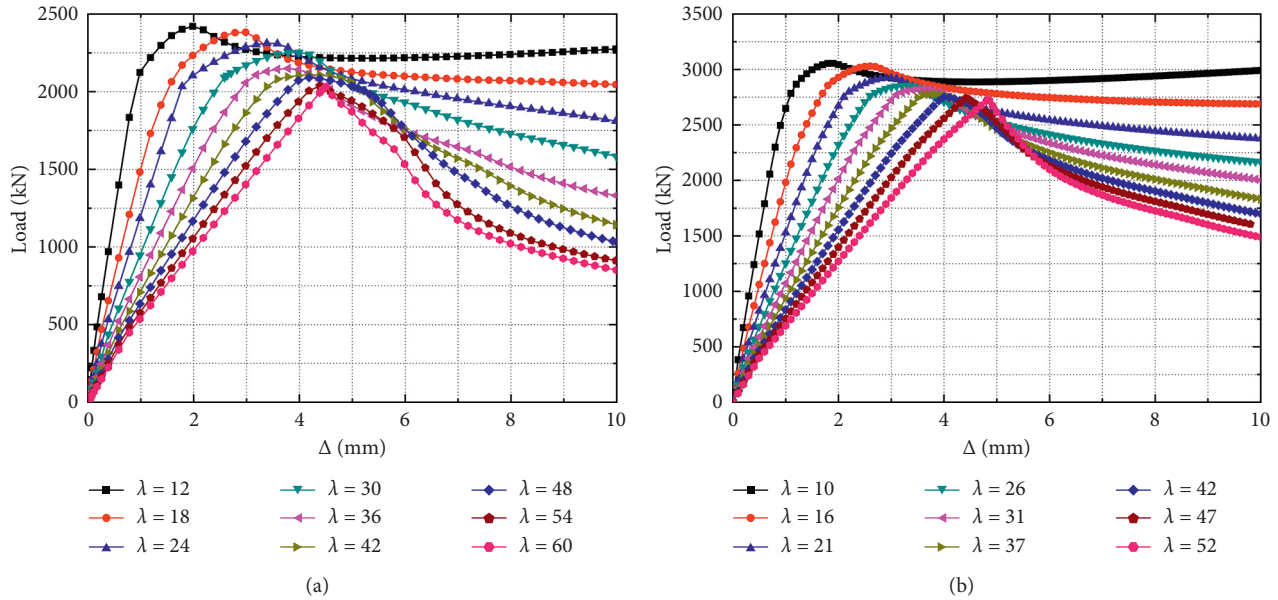

Figure 16: Load-vertical displacement curves of L/T-CFSST columns with different slenderness ratios: (a) L-shaped; (b) T-shaped.

capacity of a square CFST column is calculated under this standard as follows:

$$N_u = \frac{f_y \cdot A_s}{\gamma_s} + \frac{f_c' \cdot A_c}{\gamma_c}, \tag{6}$$

where γ_s and γ_c are the material partial factors of steel and concrete, respectively, $\gamma_s = 1.1$ and $\gamma_c = 1.5$.

The ultimate axial bearing capacity of a square CFST column is calculated under AIJ (1997) as follows:

$$N_u = 1.27A_s \cdot F + 0.85A_c \cdot f_c', \tag{7}$$

where F is the standard value of steel strength; $F = \min\{f_y, 0.7f_u\}$.

In Chinese CECS159 code, the ultimate axial bearing capacity of the square CFST column is the sum of the strength values of the steel tube and concrete:

$$N_u = f \cdot A_s + f_c \cdot A_c, \tag{8}$$

where f and f_c are the yield strength of steel and compressive strength of concrete, respectively.

The Chinese code GJB 4142-2000 adopts the unified strength theory, under which a CFST composed of two different materials (steel and concrete) is regarded as a new material. The CFST under axial compression is expressed as follows:

$$\begin{aligned} N \le \varphi \cdot N_u &= \varphi \cdot f_{sc} \cdot A_{sc}, \\ f_{sc} &= \left(1.212 + B_1 \cdot \xi_0 + C_1 \cdot \xi_0^2\right) \cdot f_c, \\ B_1 &= \left(\frac{0.1381 \cdot f}{235}\right) + 0.7646, \\ C_1 &= -\left(\frac{0.0727 \cdot f_c}{15}\right) + 0.0216. \end{aligned} \tag{9}$$

The axial bearing capacity of 72 L/T-CFSST stub columns with different section sizes was calculated to validate the above formula ($N_{u,c}$) by comparison against the FEA result ($N_{u,FEA}$) as shown in Figure 17. It is worth noting that the height of the specimen subjected to FEA is three times greater than the maximum width of the cross-section without considering the influence of the slenderness ratio.

As expected, most of the calculation results were partial to safety. The calculation results using the AIJ specification were close to the FEA values with a small discrete type. The AIJ code and effects of the confinement factor on the bearing capacity were utilized to establish a novel formula for the ultimate bearing capacity of L/T-CFSST columns after regression analysis of FEA results and test values:

$$\begin{aligned} N \le N_u &= \beta \cdot \left(A_s \cdot F + 0.85A_c \cdot f_c'\right), \\ \beta &= 0.95\left(1.1628 - 0.01459\xi\right), \end{aligned} \tag{10}$$

where N_u is the ultimate bearing capacity of L/T-CFSST stub columns, A_c is the concrete cross-sectional area, A_s is the steel tube cross-sectional area, F is the standard value of steel strength ($F = \min\{f_y, 0.7f_u\}$), f_y is the yield strength of the steel tube, f_u is the ultimate strength of the steel tube, f_c' is the cylinder compressive strength of concrete, and β is a bearing capacity increase factor obtained by regression analysis; it is related to ξ, the confinement factor. Figure 17 also shows the ultimate bearing capacity calculated by the above formula, which is very consistent with the ultimate bearing capacity obtained by FEA. In effect, the proposed formula can be used to calculate the ultimate strength bearing capacity of L/T-CFSST stub columns.

5.2. Stability Bearing Capacity. The influence of slenderness ratio is not incorporated into the formula presented above. The stability coefficient φ can be used to describe a stable column bearing capacity:

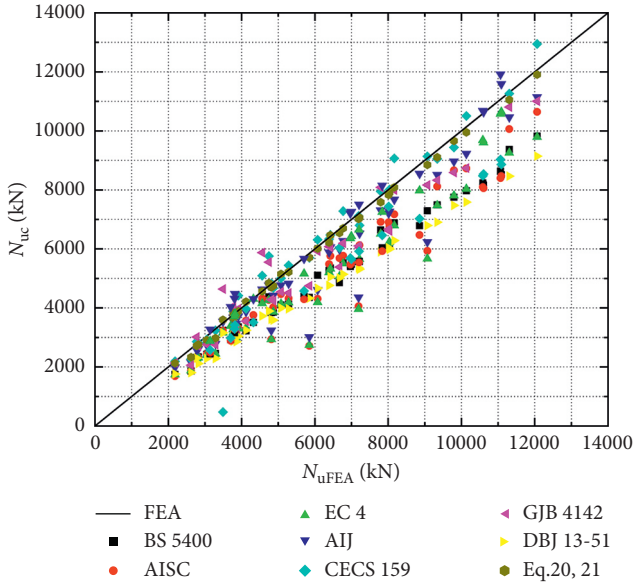

Figure 17: Comparison of FEA results against calculations from extant design codes.

$$\varphi = \frac{N_{cr}}{N_u}, \tag{11}$$

where N_{cr} is the axial stability bearing capacity of the medium-long column and N_u is the axial strength bearing capacity of the stub column. Here, 48 L/T-shaped CF ST columns with different slenderness ratios were established and analyzed to determine the functional relationship between the stability coefficient φ and slenderness ratio λ after data regression and correction:

$$\varphi = 1.0808 - 0.0062\lambda \quad 12 < \lambda_{y0} \le 60. \tag{12}$$

Above all, the bearing capacity of L/T-CFSST columns can be calculated as follows:

$$\begin{aligned} N &= \varphi N_u, \\ N_u &= \beta \cdot \left(A_s \cdot F + 0.85 A_c \cdot f_c'\right), \\ \beta &= 0.95\left(1.1628 - 0.01459\xi\right), \\ \varphi &= \begin{cases} 1, & \lambda_{y0} \le 12, \\ 1.0808 - 0.0062\lambda, & 12 < \lambda_{y0} \le 60. \end{cases} \end{aligned} \tag{13}$$

6. Conclusion

(1) The failure modes of L/T-CFSST stub columns ($H/D \le 3$) and medium-long columns ($H/D > 3$) differ. The failure mode of stub columns is characterized by the yield and local buckling of the steel tube while that of medium-long columns is attributable to the buckling and bending failure of the column. The failure mode changes from strength failure to instability failure with the increase of slenderness ratio.

(2) No weld tearing or separation of the steel tube occurred in the tests conducted here. The L/T-CFSST column shows strong mechanical properties and cooperative performance. The axial compressive process of L/T-CFSST columns can be divided into an elastic stage, elastic-plastic stage, and failure stage. The bearing capacity and ductility of the test specimens appeared to increase with steel tube thickness and strength increase and decrease as slenderness ratio increases.

(3) Calculation formulas for the axial compressive strength and stability bearing capacity of L/T-CFSST columns were established and validated according to numerical and regression analyses based on AIJ code.

Data Availability

The data used to support the findings of this study are included within the article.

Conflicts of Interest

The authors declare that they have no conflicts of interest.

Acknowledgments

This paper was supported by the Scientific Research and Development Project for Wall Material Innovation and Building Energy-Saving of Shandong Province of China (Lucaijianzhi (2014) 139).

References

[1] T. Ekmekyapar and B. J. M. Al-Eliwi, "Experimental behaviour of circular concrete filled steel tube columns and design specifications," *Thin-Walled Structures*, vol. 105, pp. 220–230, 2016.

[2] L.-H. Han, W. Li, and R. Bjorhovde, "Developments and advanced applications of concrete-filled steel tubular (CFST) structures: Members," *Journal of Constructional Steel Research*, vol. 100, pp. 211–228, 2014.

[3] L.-H. Han, W. Liu, and Y.-F. Yang, "Behaviour of concrete-filled steel tubular stub columns subjected to axially local compression," *Journal of Constructional Steel Research*, vol. 64, no. 4, pp. 377–387, 2008.

[4] L.-H. Han, S.-H. He, and F.-Y. Liao, "Performance and calculations of concrete filled steel tubes (CFST) under axial tension," *Journal of Constructional Steel Research*, vol. 67, no. 11, pp. 1699–1709, 2011.

[5] Q.-X. Ren, L.-H. Han, D. Lam, and C. Hou, "Experiments on special-shaped CFST stub columns under axial compression," *Journal of Constructional Steel Research*, vol. 98, pp. 123–133, 2014.

[6] R. Wang, L.-H. Han, and C.-C. Hou, "Behavior of concrete filled steel tubular (CFST) members under lateral impact: experiment and FEA model," *Journal of Constructional Steel Research*, vol. 80, pp. 188–201, 2013.

[7] Z.-B. Wang, Z. Tao, L.-H. Han, B. Uy, D. Lam, and W.-H. Kang, "Strength, stiffness and ductility of concrete-filled steel columns under axial compression," *Engineering Structures*, vol. 135, pp. 209–221, 2017.

[8] Z. Tao, B. Uy, F.-Y. Liao, and L.-H. Han, "Nonlinear analysis of concrete-filled square stainless steel stub columns under

axial compression," *Journal of Constructional Steel Research*, vol. 67, no. 11, pp. 1719–1732, 2011.

[9] Z. Tao, Z.-B. Wang, and Q. Yu, "Finite element modelling of concrete-filled steel stub columns under axial compression," *Journal of Constructional Steel Research*, vol. 89, pp. 121–131, 2013.

[10] Q.-X. Ren, L.-H. Han, C. Hou, Z. Tao, and S. Li, "Concrete-encased CFST columns under combined compression and torsion: Experimental investigation," *Journal of Constructional Steel Research*, vol. 138, pp. 729–741, 2017.

[11] E. M. Güneyisi, A. Gültekin, and K. Mermerdaş, "Ultimate capacity prediction of axially loaded CFST short columns," *International Journal of Steel Structures*, vol. 16, no. 1, pp. 99–114, 2016.

[12] F. Abed, M. AlHamaydeh, and S. Abdalla, "Experimental and numerical investigations of the compressive behavior of concrete filled steel tubes (CFSTs)," *Journal of Constructional Steel Research*, vol. 80, pp. 429–439, 2013.

[13] X. Liu, C. Xu, J. Liu, and Y. Yang, "Research on special-shaped concrete-filled steel tubular columns under axial compression," *Journal of Constructional Steel Research*, vol. 147, pp. 203–223, 2018.

[14] Z. Wang, Z. H. Chen, and Q. Q. Xiong, "Performance of L-shaped columns comprising concrete-filled steel tubes under axial compression," *Journal of Constructional Steel Research*, vol. 145, pp. 573–590, 2018.

[15] M. Lei, Z. Y. Shen, Y. Q. Li, and J. H Luo, "Behavior of concrete-filled T-shaped steel tube intermediate long columns subjected to axial loading," *Journal of Tongji University (Natural Science)*, vol. 44, no. 4, pp. 520–527, 2016, in Chinese.

[16] Y. Chen, Z. Y. Shen, M. Lei, and Y. Q. Li, "Experimental investigation on concrete-filled T-shaped steel tube stubs subjected to axial compression," *Journal of Tongji University (Natural Science)*, vol. 44, no. 6, pp. 822–829, 2016, in Chinese.

[17] Z.-Y. Shen, M. Lei, Y.-Q. Li, Z.-Y. Lin, and J.-H. Luo, "Experimental study on seismic behavior of concrete-filled L-shaped steel tube columns," *Advances in Structural Engineering*, vol. 16, no. 7, pp. 1235–1247, 2013.

[18] Z.-L. Zuo, J. Cai, C. Yang, Q.-J. Chen, and G. Sun, "Axial load behavior of L-shaped CFT stub columns with binding bars," *Engineering Structures*, vol. 37, pp. 88–98, 2012.

[19] Z.-L. Zuo, J. Cai, C. Yang, and Q.-J. Chen, "Eccentric load behavior of L-shaped CFT stub columns with binding bars," *Journal of Constructional Steel Research*, vol. 72, pp. 105–118, 2012.

[20] Z.-L. Zuo, J. Cai, Q.-J. Chen, X.-P. Liu, C. Yang, and T.-W. Mo, "Performance of T-shaped CFST stub columns with binding bars under axial compression," *Thin-Walled Structures*, vol. 129, pp. 183–196, 2018.

[21] Y.-T. Wang, J. Cai, and Y.-L. Long, "Hysteretic behavior of square CFT columns with binding bars," *Journal of Constructional Steel Research*, vol. 131, pp. 162–175, 2017.

[22] L. H. Xu, G. F. Du, F. Wen, and H. R. Xu, "Experimental study on normal section compression bearing capacity of composite T-shaped concrete-filled steel tubular columns," *China Civil Engineering Journal*, vol. 42, no. 6, pp. 14–21, 2009, in Chinese.

[23] L. L. Liu, Y. Q. Tu, and Y. H. Ye, "Experimental study of the properties of axially loaded multi-cell T-shaped concrete-filled steel tubular stub columns," *China Civil Engineering Journal*, vol. 44, no. 10, pp. 9–16, 2011, in Chinese.

[24] Y. Q. Tu, Y. F. Shen, and P. Li, "Behaviour of multi-cell composite T-shaped concrete-filled steel tubular columns under axial compression," *Thin-Walled Structures*, vol. 85, pp. 57–70, 2014, in Chinese.

[25] Y. Sui, Y. Tu, Q. Guo, J. Zhang, and F. Ke, "Study on the behavior of multi-cell composite T-shaped concrete-filled steel tubular columns subjected to compression under biaxial eccentricity," *Journal of Constructional Steel Research*, vol. 159, pp. 215–230, 2019.

[26] Y. Q. Tu and Q. S. Wen, "Bearing capacity calculation of L-shaped concrete filled steel tubular columns subjected to axial compression," *Journal of Building Structures*, vol. 34, no. S1, pp. 314–320, 2013.

[27] Y. L. Yang, H. Yang, and S. M. Zhang, "Compressive behavior of T-shaped concrete filled steel tubular columns," *International Journal of Steel Structures*, vol. 10, no. 4, pp. 419–430, 2010.

[28] C. Xu, Y. Yang, X. Tang, and J. Liu, "Experimental research on static behavior of stiffened T-shaped concrete-filled steel tubular stubs subjected to concentric axial loading," *International Journal of Steel Structures*, vol. 19, no. 2, pp. 591–602, 2018.

[29] Q. Xiong, Z. Chen, W. Zhang, Y. Du, T. Zhou, and J. Kang, "Compressive behaviour and design of L-shaped columns fabricated using concrete-filled steel tubes," *Engineering Structures*, vol. 152, pp. 758–770, 2017.

[30] T. Zhou, M. Y. Xu, M. Y. Xu et al., "Eccentric loading behavior of L-shaped columns composed of concrete-filled steel tubes," *Advanced steel construction*, pp. 227–244, The Hong Kong Polytechnic University, Hung Hom, Hong Kong, 2016.

[31] Q. Xiong, Z. Chen, J. Kang, T. Zhou, and W. Zhang, "Experimental and finite element study on seismic performance of the LCFST-D columns," *Journal of Constructional Steel Research*, vol. 137, pp. 119–134, 2017.

[32] Y. Du, Z. Chen, Y.-B. Wang, and J. Y. Richard Liew, "Ultimate resistance behavior of rectangular concrete-filled tubular beam-columns made of high-strength steel," *Journal of Constructional Steel Research*, vol. 133, pp. 418–433, 2017.

[33] M. Xu, T. Zhou, Z. Chen, Y. Li, and L. Bisby, "Experimental study of slender LCFST columns connected by steel linking plates," *Journal of Constructional Steel Research*, vol. 127, pp. 231–241, 2016.

[34] T. Zhou, M. Xu, X. Wang, Z. Chen, and Y. Qin, "Experimental study and parameter analysis of L-shaped composite column under axial loading," *International Journal of Steel Structures*, vol. 15, no. 4, pp. 797–807, 2015.

[35] L. H. Han, *Concrete-filled Steel Tubular Structures-Theory and Practice (Third Version)*, China Science Press, Beijing, China, 2007, in Chinese.

[36] American Concrete Institute, *Building Code Requirements for Structural Concrete and Commentary (ACI-318R 2005)*,American Concrete Institute, Farmington Hills, MI, USA, 1997.

[37] F.-C. Wang and L.-H. Han, "Analytical behavior of special-shaped CFST stub columns under axial compression," *Thin-Walled Structures*, vol. 129, pp. 404–417, 2018.

[38] British Standards Institution, *Steel, Concrete and Composite Bridges—Part 1: General Statement (BS 5400)*, British Standards Institution, London, UK, 1998.

[39] American National Standard, *Specification for Structural Steel Buildings (ANSI/AISC 360-05)*, American National Standard, New York, NY, USA, 2005.

[40] Design of Composite Steel and Concrete Structures-Part1-1, General Rules-Structural Fire Design (Eurocode 4).

[41] Architectural Institute of Japan, *Recommendations for Design and Construction of Concrete Filled Steel Tubular Structures*, AIJ, Tokyo, Japan, in Japanese, 1997.

[42] CECS, *Technical Specifications for Structures with Concrete-Filled Rectangular Steel Tube Members*, CECS, China Planning Press, Beijing, China, 2014, in Chinese.
[43] Technical specifications for early-strength model composite structure used for navy port emergency repair in wartime, (GJB 4142-2000), in Chinese.
[44] Technical specifications for concrete filled steel tubular structures (DBJ/T13-51-2010), in Chinese.